



Seismic Hazard of American Samoa and Neighboring South Pacific Islands: Methods, Data, Parameters, and Results

By Mark D. Petersen, Stephen C. Harmsen, Kenneth S. Rukstales, Charles S. Mueller, Daniel E. McNamara, and
Melanie Walling

Report Series XXXX–XXXX

U.S. Department of the Interior
U.S. Geological Survey

U.S. Department of the Interior
KEN SALAZAR, Secretary

U.S. Geological Survey
Marcia K. McNutt, Director

U.S. Geological Survey, Reston, Virginia 200x
Revised and reprinted: 200x

For product and ordering information:
World Wide Web: <http://www.usgs.gov/pubprod>
Telephone: 1-888-ASK-USGS

For more information on the USGS—the Federal source for science about the Earth,
its natural and living resources, natural hazards, and the environment:
World Wide Web: <http://www.usgs.gov>
Telephone: 1-888-ASK-USGS

Suggested citation:

Petersen, Mark D., Harmsen, Stephen c., Rukstales, Kenneth S., Mueller, Charles, S., McNamara, Daniel E., and Walling, Melanie, Seismic hazard of American Samoa and neighboring South Pacific Islands: methods, data, parameters, and results, U.S. Geological Survey Open-file report, Denver, CO.

Any use of trade, product, or firm names is for descriptive purposes only and does not imply endorsement by the U.S. Government.

Although this report is in the public domain, permission must be secured from the individual copyright owners to reproduce any copyrighted material contained within this report.

Contents

Abstract	1
Introduction.....	2
Methodology	3
Seismic Source Model.....	6
Ground Motion Model.....	11
Logic Tree for Seismic Hazard	14
Results.....	15
Conclusions	16
References Cited.....	17
Acknowledgements	20
Appendix A: Lessons of the Samoa from the M8.3 Tokachi-Oki and the M9 Tohoku Earthquakes	21

Figures

No table of figures entries found.

Tables

1. Table of GSN data.....	Error! Bookmark not defined.
1. Table of Earthquake ground motions for islands.....	Error! Bookmark not defined.

Seismic Hazard for American Samoa and Neighboring South Pacific Islands: Data, Methods, Parameters, and Results

By Mark D. Petersen, Stephen C. Harmsen, Kenneth S. Rukstales, Charles S. Mueller, Daniel E. McNamara, and Melanie Walling

Abstract

American Samoa has experienced numerous earthquakes that have caused significant effects from ground shaking and tsunamis. To mitigate earthquake risks from ground shaking, the Federal Emergency Management Agency (FEMA) requested that the USGS develop seismic hazard maps for ground shaking that could be applied in building design criteria. This Open-file report describes the data, methods, and parameters used to calculate the seismic shaking hazard as well as the output hazard curves and deaggregation information needed for building design. Spectral acceleration hazard for 1 Hz having a 2% probability of exceedance on a firm rock site condition is 0.15 g (1 Hz) and 0.54 g (5 Hz) at a site on American Samoa, 0.89 g (1 Hz) and 3.28 g (5 Hz) at a site on Tonga, 0.18 g (1 Hz) and 0.71 g (5 Hz) at a site on Fiji, and 0.96 g (1 Hz) and 3.25 g (5 Hz) at a site on the Vanuatu Islands.

Introduction

The American Samoa region is located in a complex tectonic zone that includes earthquakes on the subduction interface, within the subducting slab, outer rise, and along other fractures, spreading centers, and shear zones distributed across the region. Seismicity and geodesy observation indicate rapid deformation rates. Figure 1 (Pelletier and others, 1998) shows some of the deformation rates and locations of large $M > 7$ earthquakes. Large earthquakes are common within this rapidly deforming region with 242 $M \geq 7$ (198 declustered $M \geq 7$) earthquakes included in our catalog since 1900.

For this hazard assessment we considered four published ground motion prediction equations for assessing ground shaking levels (Youngs and others 1997-Geomatrix; Atkinson and Boore, 2003, and Zhao and others, 2006) from subduction interface and deep intraslab earthquakes. We tested each ground motion prediction equations to determine their applicability for this region using Global Seismic Network (GSN) strong motion data from large earthquakes that we processed and that were not used in developing these ground motion models.

In this paper we describe the development of hazard maps for this region that will be provided to building code committees for their analysis of American Samoa design procedures. The USGS has developed hazard maps over the past 35 years that are applied in seismic provisions for construction such as the NEHRP Recommended Provisions for Seismic Regulations, Minimum Design Loads for Building and Other Structures ASCE-7 code, and the International Building Code (e.g., Algermissen and Perkins, 1976; Frankel and others, 2002; and Petersen and others, 2008). In this study we apply similar methodologies for developing hazard maps of the South Pacific region. We have expanded the study region to include other South Pacific islands because only a few small-scale seismic-hazard maps have been developed for this region (e.g. the Global Seismic Hazard Assessment Program (GSHAP; Guarding, 1999) and because our results show that the earthquakes across this region have similar

source and ground shaking characteristics. We compare our results to Suckale and Grünthal (2009) recently developed probabilistic seismic hazard model for Vanuatu. This analysis is for seismic shaking only and does not include a probabilistic tsunami hazard model. For information on tsunami inundation limits of the September 29, 2009 tsunami on Tutila, American Samoa we refer the reader to a USGS report by Jaffe et al., 2010.

Methodology

We apply the same hazard calculation methodology that was used in developing the National Seismic Hazard Maps for the Conterminous U.S. and Alaska (Frankel and others, 2002; Petersen and others, 2008). Probabilistic hazard is calculated by developing models of seismicity-derived gridded-background sources, models of earthquakes on faults, and models of ground shaking resulting from these earthquakes. We include two different classes of earthquake source models in these maps: (1) smoothed-gridded seismicity and (2) subduction fault sources. The seismicity models are based on the earthquake catalog and characterize the hazard from earthquakes between about M5.0 and M7.0 or an alternative maximum magnitude inferred from the historic earthquake catalog. The model assumes subduction interface sources from M 7.0 to a maximum magnitude based on historic seismicity or global analogs. We consider earthquakes with depths close to the surface down to 700 km.

Gridded Seismicity Sources

Random seismicity-derived background sources account for two types of earthquakes: those that occur off known faults, and moderate- size earthquakes that are not modeled on faults. This model is based on an earthquake catalog, which is constructed by merging catalogs developed by different institutions. Duplicate events and manmade events are deleted. Seismicity models require a declustered

earthquake catalog of independent events for calculation of Poissonian (time-independent) earthquake rates. Therefore, the catalog is declustered to remove dependent events such as foreshocks or aftershocks. Completeness levels are estimated from the earthquake catalog and regional b-values (from Gutenberg and Richter, 1944) are computed using a maximum likelihood method (Weichert, 1980). Gridded-seismicity background models are based on smoothed seismicity $M \geq 4$ using a two-dimensional Gaussian smoothing operator (Frankel, 1995) from which earthquake rates (10^a values from the Gutenberg and Richter relationship) are calculated over a grid. This model accounts for the observation that larger earthquakes occur at or near clusters of previous smaller earthquakes (Frankel, 1995).

To calculate the hazard from gridded-seismicity background sources, we apply a truncated-exponential, Gutenberg-Richter magnitude-frequency distribution (Gutenberg and Richter, 1944). The hazard is calculated using a minimum magnitude of 5.0 up to some maximum magnitude. Maximum magnitude values are determined from paleoseismic information, historical seismicity, or global analogy. Zones allow for local variability in seismicity characteristics or plate tectonics. This variability incorporates alternative models of the b-value or the maximum magnitude - M_{max} . The hazard is calculated for potential earthquakes at each grid cell. Earthquakes smaller than $M 6.0$ are characterized as point sources at the center of each cell, whereas earthquakes larger than $M 6.0$ assume hypothetical finite vertical or dipping faults centered on the source grid cell. To calculate lengths from a particular magnitude, we precalculate average distances from virtual faults with strike directions uniformly distributed from 0 to 180° (Appendices B and C in Petersen and others 2008). The average-distance calculation ensures that no receiver is assigned a biased distance based on an arbitrary draw from a random-number generator. The virtual fault length is based on a subduction-zone earthquake rupture length versus magnitude regression performed by Youngs and others (1997) The formula is:

$$\text{rupture length} = 10^{(M-4.94)/1.39}.$$

Subduction Fault Sources

Earthquake recurrence rates and geometry for subduction faults are based on geologic measurements, geodesy strain rates, and seismicity characteristics. An important consideration in the hazard analysis is estimating the sizes of earthquakes that can rupture along the subduction interfaces of the Tonga and New Hebrides zones. We estimate the a and b -values along a fault by fitting a Gutenberg-Richter (Gutenberg and Richter, 1944) magnitude-frequency distribution to the historic seismicity. Alternative source models are then constructed for estimating the epistemic uncertainty in the maximum magnitude that is capable of occurring in the zone. This uncertainty is described using logic-trees that characterize alternative input models and their weights at each decision point in the analysis (epistemic uncertainty). Aleatory variability (random variability) is considered directly in the seismic hazard code and considers variability in the locations and magnitudes of future earthquakes along the subduction zones. Typically a given parameter contains both epistemic uncertainty and aleatory variability components.

Attenuation Relations

Ground-motion prediction equations or attenuation relations relate the source characteristics of the earthquake and propagation path of the seismic waves to the ground motion at a site. The predicted ground motion is typically quantified in terms of a median value which is a function of magnitude, distance, style of faulting, and other factors. These models assume a lognormal probability density function of peak horizontal ground acceleration or spectral accelerations that are used in calculating the probability of exceedance. In this hazard model we generally calculate ground motions from subduction interface sources that are up to 1,000 kilometers and intraslab earthquake that are up to 200 km (epicentral distance) from the site. We apply the subduction interface models to account for large

shallow earthquakes less than 50 km on the subducting fault plane and intraslab earthquakes to characterize all other earthquakes. The ground motion alternative models are accounted for in a logic tree framework to account for epistemic uncertainty. Random aleatory variability is accounted for directly in the seismic hazard code and this variability is integrated to obtain the probability of exceedance of a particular ground motion level.

Seismic Source Model

In the seismic source model we consider earthquakes associated with the subduction interface, intraslab (or inslab) earthquakes that extend to 700 km depth, and background seismicity that accounts for geologic structures that are not modeled explicitly. The seismic source model is composed of two subduction source models and background source models for different depth layers, tectonic regimes, and maximum magnitudes. We are not aware of slip rate data or paleoseismic studies for faults on these South Pacific islands. Therefore, the earthquakes on subduction zone faults and background seismicity are modeled using historic seismicity. This hazard model assumes that earthquakes will continue at the same rate and size distribution as observed over the past century.

Earthquake catalog

A new seismicity catalog was compiled for this project from three global source catalogs. The Engdahl and Villaseñor (2002) catalog (EVC) includes earthquakes greater than about magnitude 6.5 since 1900 and about magnitude 5.5 since 1964. A second catalog (PDE) was downloaded from the USGS Earthquake Hazards Program website including earthquakes from 1973 through December 2010 (http://earthquake.usgs.gov/earthquakes/eqarchives/epic/epic_rect.php, “Rectangular Area Search”, accessed 06 January 2011). A third catalog (ISC) was downloaded from the International Seismological

Centre website including earthquakes from 1907 through May 2008

(<http://www.isc.ac.uk/search/bulletin/rectang.html>, “On-line Bulletin, Rectangular Selection”, accessed 26 July 2010). The three source catalogs were reformatted, concatenated, and sorted chronologically. Moment magnitudes (M_w) were either selected directly from original source catalogs or converted from other magnitude types using published relations that account for saturation and other scaling effects; we use Sipkin (2003) to convert m_b to M_w , and bilinear or trilinear approximations to the curves plotted by Utsu (2002) for M_s and m_L . Duplicate catalog entries were identified and deleted using the preference order: EVC > PDE > ISC. For the hazard analysis, foreshocks and aftershocks were identified and deleted using the declustering methodology of Gardner and Knopoff (1974). No special declustering treatment was applied for great earthquakes. The Gardner and Knopoff technique only considers earthquakes up to magnitude 8, using a maximum 94-km-radius circular aftershock window. In our implementation, however, aftershocks of aftershocks are deleted, so a natural expansion of the declustered region can occur for a very large event.

Figure 4 shows the annual rate of earthquakes with magnitudes between M 4 and M 9 for earthquakes since 1900 and 1964 as well as the declustered catalogs from the same periods. The earthquakes follow a Gutenberg-Richter magnitude frequency distribution (Gutenberg and Richter, 1944) between M 5 and the upper magnitudes; for earthquakes with magnitudes less than M 5 the curve bends over suggesting an incomplete catalog. Therefore, we use M 5.0 as our completeness cutoff for the earthquake catalog in the model. For calculating the gridded background seismicity sources we consider the catalog that contains events since 1964. Most of the declustering occurs for earthquakes less than M 7. The rates calculated for the 1900 and 1964 catalogs are similar for events greater than M 6.5.

Gridded-Seismicity Background Model

We use the declustered catalog as the basis for the background source model. The $M \geq 4$ earthquakes since 1964 are smoothed using a 50 km smoothing kernel and $10^{(a)}$ values (from Gutenberg-Richter) are calculated at grid points spaced 0.1 degree apart in longitude and latitude. We calculate the b-values based on the 1900-2010 and 1964-2010 catalogs for several regions and depth intervals (Figures 5 and 6). With one exception the calculated b-values are generally close to 1.0 for the background and outer rise zones but we use the calculated b-values in this hazard analysis (Table 1). The primary outlier in this b-value analysis is associated with the zone overlying the upper 50 km of the New Hebrides subduction zone where the b value is about 0.58. We use the calculated a and b-values to produce a magnitude-frequency distribution from M 5.0 to Mmax. The seismicity analysis of Sukale and Grünthal (2009) indicates a b-value of 0.71. They use a different declustering algorithm, so this would, most likely account for some of the difference.

Subduction Zone Earthquake Source Model

Subduction-interface earthquakes $M \geq 7$ are considered as rupturing from 10 km down to 50 km depth. Deeper earthquakes on the Wadati-Benioff zone are modeled as gridded seismicity models using a Gutenberg and Richter (1944) magnitude frequency distribution with the smoothed rate of earthquakes and a calculated b-value. Figure 7 shows a magnitude-frequency plot of the 32 shallow $M \geq 7$ earthquakes associated with the New Hebrides zone. The b-value of 0.58 that was calculated from the $M \geq 4$ earthquakes does not fit the rates of the larger earthquakes. We apply a b-value of 1.0 to predict earthquakes $M \geq 7$ events in the model. Figure 8 shows a magnitude-frequency plot of the 22 $M \geq 7$ earthquakes associated with the Tonga subduction zone. The b-value calculated for $M \geq 4$ earthquakes in this region is consistent with the b-values calculated from $M \geq 7$ earthquakes within the Tonga zone so

we use the calculated b-value of 0.87 for the entire range of earthquakes from M 5.0 to 7.0. The slip rate varies along the strike of the New Hebrides and Tonga subduction zones so we considered whether or not to allow for variable rates of $M \geq 7$ events. Figure 1 shows $M \geq 7$ earthquakes and the observed rate of earthquakes does not appear to be correlated with the slip rate variability. For example, of the 32 $M \geq 7$ events along the New Hebrides zone 17 occurred along the northern half of the zone and 15 along the southern half of the zone, even though the slip rate varies significantly along the strike (Fig. 1). Of the 22 $M \geq 7$ earthquakes along the Tonga zone 12 events occurred in the northern half and 10 events in the southern half of the zone, even though slip rates displayed in Figure 1 in the northern portion of the zone are more than double slip rates in the southern portion of the zone. Moreover, the seismicity appears to be located uniformly along the length of these zones, although the Tonga zone exhibits less uniformity and contains two clusters of large earthquakes, one cluster is located in the far north and one in the southern portion of the zone. Therefore, for this assessment we assume that the seismicity rate does not vary along the strike of the subduction zone and is consistent with the historic rate of earthquakes along the entire zone.

Earthquakes occurring prior to modern seismic instrumentation were sometimes recorded from written observations of tsunamis or earthquake effects. Okal and others (2004) suggest that three large earthquakes in the early twentieth century on the Tonga-Kermadec arc system were thought to have maximum magnitudes between 8.4 and 8.7. They suggest that more recent moment estimates of these events led to the perception that maximum magnitude for earthquakes on this subduction zone would have moment of 2.5×10^{28} dyne-cm, which is consistent with a lower Mw 8.2 earthquake. Okal and others (2004) interpreted regional tsunami data from the November 17, 1865 earthquake as originating from a large earthquake on the Tonga-Kermadec arc system with moment of 4×10^{28} , which is consistent with Mw 8.4. This evidence in combination with the December, 2004 M 9.1 earthquake on

the Sumatra subduction zone and the March, 2011 M 9.0 earthquake near Sendai on the Japan subduction zone (both events were greater in size than anticipated) were influential in assessing the alternative maximum magnitude models that we applied to these subduction zones. We have assigned a weight of $\frac{1}{2}$ to the model in which these earthquakes occur with magnitude up to 8.5 and a weight of $\frac{1}{2}$ to the model in which these earthquakes are capable of rupturing in earthquakes up to magnitude 9.0 on the subduction interface. For all other zones we typically have considered the largest historic magnitude with an additional 0 to 0.2 magnitude units to account for the possibility that we have not observed the largest potential earthquake during the past century. Table 1 shows the largest observed earthquakes in each zone as well as the applied maximum magnitude.

Subduction Zone Source Geometry

Figure 9 shows the source zones considered for our model. We separated out 5 zones in the model: (1) Tonga subduction interface, (2) New Hebrides subduction interface, (3) Tonga outer rise, (4) New Hebrides outer rise, (5) the Fiji zone that encompasses much of the back-arc spreading and fracture zones in the Fiji platform, and (5) all the other areas not considered in the previous zones. The geometry of the Tonga and New Hebrides subduction-interface models is based on the Slab 1.0 model of Hayes and others (2011) which applies bathymetry, seismicity, and reflection profile data to constrain the three-dimensional non-planar geometry of subduction zones from the trenches through the base of the seismogenic layer. We define the interface zones above the 10 km to 50 km depth contours defined by the Slab 1.0 model. It is clear that some of the seismicity included above this depth interval is not on the interface but may have ruptured within the slab. It would be helpful in the future to define a 3-d zone or analyze the focal mechanisms to better differentiate the interface and intraslab earthquakes. The Outer Rise zone parameters were based on the location of the normal fault earthquakes on the leading

edge of the subducting slab, in the region where the slab bends due to frictional resistance as the tectonic plate descends. The ends of the outer rise zones are defined at the end of the mapped subduction zones of Pelletier and others (1998) and Bird (2003; Figure 1). The northern boundary of the Tonga zone was defined along a lineament of seismicity that extends southwest across the map. Seismicity is much sparser to the north of that zone. The Fiji zone outlines the Fiji platform which can be observed in the bathymetry data and is defined many of the geologic structures shown by Pelletier and others (1998) and Bird (2003).

Ground Motion Model

Ground motion prediction equations that model the ground motion from intraslab (intraplate) earthquakes and plate interface earthquakes have been developed by Atkinson and Boore (2003), Youngs and others (1997)-Geomatrix, and Zhao and others (2006). These models were used in the U.S. National Seismic Hazard Maps (Petersen and others, 2008) and they are the ground motion models considered in this study. Each ground motion model of ground motions from intraslab earthquakes has terms that allow for increased ground motion with depth; however, their estimates of the motion are not well constrained for depths below 200 km because strong motion data at deeper depths was not typically considered in developing the prediction equations. Atkinson and Boore (2003) and Zhao and others (2006) recommend that the ground motions should not continue to increase for earthquakes with depths greater than 100 km or 125 km, respectively. Therefore, we limited the intraslab ground motions obtained from the Atkinson and Boore (2003) equations from growing when the earthquakes occur at depths below 100 km. Similarly, we have limited the intraslab ground motions obtained from the other two equations from growing when the earthquakes occur at depths below 125 km. Future studies should focus on ground motions with depths deeper than 200 km.

Figures 10 through 12 show primary features of the ground motion models and illustrate how ground motion decays as a function of distance, magnitude, mechanism of earthquake, and depth. Figures 10 and 11 show the four ground motion prediction equations for 1 Hz and 5 Hz spectral acceleration from earthquakes with different magnitudes and for interface and intraplate earthquakes. Typically intraslab earthquake ground motions for M 7.5 are greater than the ground motions from similar size events occurring on the plate interface at distances less than 100 km, for both 1 Hz and 5 Hz spectral acceleration models. Figure 12 shows how these ground motions vary with the earthquake depth. For M 7.5 earthquake, the ground motions are typically reduced for deeper earthquakes out to about 50 km epicentral distance. At larger epicentral distances the curves cross over and deeper earthquakes can generate similar or larger ground motions.

Figure 13 shows the earthquakes and Global Seismic Network (GSN) strong motion stations that recorded those earthquakes at distances less than 1000 km. We included strong motion records from 9 stations shown in Table 2. Figures 14 and 15 show comparisons of the geometric mean for 1 Hz and 5 Hz spectral accelerations. We normalized the ground motions to a common depth of 30 km and to the nearest 0.5 magnitude using the terms from Youngs and others (2005). In general, these strong motion data (not considered in developing the models) appear to be compatible with the intraslab ground motion prediction equations.

We calculated the residuals (natural log of the observed ground motion subtracted from the predicted ground motions) using GSN strong motion data that was not used in developing any of the ground motion prediction equations. The purpose of this residual study was to test if these global ground motion equations predicted ground motions that were consistent with the observed strong motions that were recorded in the Samoa and similar regions (Figure 16). For 1 Hz and 5 Hz spectral ground motions the Atkinson and Boore (2003) equations and the Zhao and others (2006) relation generally

underpredict the observed ground motions while the Youngs and others (1997)-Geomatrix equation overpredicts the ground motions at magnitudes less than 7.5.

Figure 17 shows how the residuals vary by station with the number of station records shown in parentheses. The data most likely contain station correlations so we examined the strong motion records for each station to see if there were any regional or station specific correlations that we could identify. In general we do not see any particular region of the circum-Pacific varying systematically. However, strong motion data recorded at station RAO (near the Kermadec trench) were typically higher than the predicted values. Additional examination of strong motion records from RAO did not lead us to exclude these recordings. However, descriptions of station RAO indicate that it is located near the edge of a small island with a 200 foot cliff. Therefore, it is likely that its records include topographic amplifications. In general, stations from Alaska to American Samoa appear to have normally distributed variability and do not appear to be significantly biased either higher or lower than the median ground motion prediction equation. Correlations of the site effects from different stations should be considered explicitly, since the data are not sampled evenly across the Pacific region. However, for this study we assume that some of the stations will record above average ground motions and others record lower than average ground motions but that as a group they should provide a reasonable estimate of the mean ground motion residuals.

Weights of the ground motion models were based on the residual analysis discussed above (Figure 18). The Zhao and others (2006) model overall had the lowest residuals so we assigned weights that were slightly higher for that model. The Zhao and others (2006) and Atkinson and Boore (2003) models often under predict the ground motions so we assigned some weight to the Youngs and others (1997)/Geomatrix model that predicts higher than observed ground motions. The two Atkinson and Boore models are quite similar, especially at 1 s spectral acceleration and we gave similar weight to the

two equations for global and Cascadia subduction earthquakes and together their summed weight is similar to the weight assigned to the Zhao and others (2006) model. The weighted combination of these predicted ground motion residuals in a logic tree (Figure 18) for M 7 earthquakes at 1 Hz spectral acceleration results in ground motion residuals near zero.

Logic Tree for Seismic Hazard

The final logic tree that we used for this hazard analysis is shown in Figure 18. Branches of the logic tree are shown for magnitude uncertainty and ground motion models. As discussed in the source model section, we considered earthquakes with a maximum magnitude of 8.5 or 9.0. This decision does not make a large impact on the ground motions with M 9.0 model being higher by about 5% to 10%. The implied slip rate from our model with maximum magnitude of 8.5 is about 4.5 cm/yr for the New Hebrides subduction and about 2.5 cm/yr for the Tonga Subduction Zone. The rate for the model with maximum magnitude of 9.0 is about 9.5 cm/yr for the New Hebrides Subduction Zone and about 5 cm/yr for the Tonga Subduction Zone. These implied slip rates account for less than half of the total slip rates shown in Figure 1. For the ground motion models we assigned weights as described above based on the residual analysis. Alternative weights were assigned for ground motion models from earthquakes with depths down to 200 km and for earthquakes located at greater depths based on the residual analysis. We found that ground motions from earthquakes at 10 km to 200 km depth had similar characteristics.

Results

The relative contributions of each source to the overall ground motion hazard is displayed in Figures 19 and 20. Ground motions near the Wadati-Benioff zone dominate the hazard. Ground motion hazard is highest for the shallowest seismicity and hazard tends to decrease with depth. It is important to point out that the ground motions associated with deep earthquakes have not been studied well. Future work and data may help us better constrain this shaking from deep earthquakes that has caused light damage over broad areas (e.g., 1994 M 8.2 Bolivia earthquake, 642 km deep caused limited damage).

Spectral accelerations at 1 Hz (1 s) and 5 Hz (0.2 s) and peak horizontal ground motion hazard maps (with 5% damping) for this South Pacific region at 10% and 2% probabilities of exceedance in 50 years on a uniform firm rock site condition are shown in Figures 21 to 26. For assessment of site specific hazard it is critical that further studies should consider local faulting and ground motion amplification. These hazard maps were only produced for a single $V_{s30} = 760$ m/sec site condition so these hazard values need to be modified for appropriate site effects.

The probabilistic seismic hazard model for Vanuatu developed by Suckale and Grünthal (2009) provides lower estimates of hazard than the model presented here. The Suckale and Grünthal (2009) model for peak ground acceleration on stiff soil at Port Vila, Vanuatu is about 0.7g for a 10% probability of exceedance in 50 year level. If we assume that the stiff soil is consistent with a shear wave velocity in the upper 30 m (V_{s30}) of 360 m/s, then we would calculate a pga hazard of 0.9 g which is about 30% higher than theirs. Comparison of the 0.2 s and 1 s spectral accelerations under these same assumptions of soil amplification also indicate that our values are significantly higher than the model developed by Suckale and Grünthal (2009). This difference could be related to the different suite of attenuation relations we apply or that we have misinterpreted their soil classification. We also

use a higher maximum magnitude for the New Hebrides subduction zone than was applied in their hazard assessment.

Disaggregation information for four sites: Pago Pago, American Samoa; Nuku'alofa, Tonga; Suva, Fiji, and Port Vila, Vanuatu is shown in Figures 27 to 38. Figures 27 to 30 show bar charts that describe the primary contributors to the hazard along with the modal magnitude, distance, and epsilon (difference of the calculated ground motion from the median ground motion) that contributes most to the hazard. For the American Samoa site, M 7.0 to 7.4 earthquakes at distances about 70 km on the Tonga outer rise are most important to the hazard but large subduction interface earthquakes with magnitudes of about M 8.4 at large distances of 280 km are also significant. For the site in Tonga the M 7.5 earthquakes at distances of 38 km located on the shallow Fiji platform contributes most to the hazard but the large subduction interface and Wadati-Benioff earthquakes are also significant. At the Fiji site, the Fiji platform and Wadati-Benioff earthquakes with magnitudes about M 8.0 and distances close to 100 km dominate the seismic hazard. For the Vanuatu site several sources contribute to the hazard including the New Hebrides interface and shallow Fiji platform earthquakes. A broad range of magnitudes from 6.3 to 8.7 are important contributors with modal distances for the earthquakes that contribute most to the hazard range from 30 km to 114 km. Figure 31 to 38 show graphs of the closest distance, magnitude, and epsilon as well as geographic disaggregations showing the locations of the important sources. For most of these sites the high rates of earthquakes included in the source model lead to epsilons greater than the median value.

Conclusions

The hazard across the region varies significantly. Spectral acceleration hazard for 1 Hz having a 2% probability of exceedance on a firm rock site condition is 0.15 g (1 Hz) and 0.54 g (5 Hz) at a site on American Samoa, 0.89 g (1 Hz) and 3.28 g (5 Hz) at a site on Tonga, 0.18 g (1 Hz) and 0.71 g (5 Hz) at

a site on Fiji, and 0.96 g (1 Hz) and 3.25 g (5 Hz) at a site on the Vanuatu Islands. If the site is located on something other than firm rock ($V_{s30}=760$ m/s) it is important to amplify the hazard by a factor consistent with the soil or rock located at the site. NEHRP has developed factors for this purpose.

References Cited

- Atkinson G.M., and D. M. Boore, 2003, Empirical ground-motion relations for subduction-zone earthquakes and their application to Cascadia and other regions, *Bull. Seismol. Soc. Amer.*, v 96, p 1703-1729.
- Bevis, M., F.W. Taylor, B.E. Schutz, J. Recy, B.L. Isacks, S. Helu, R. Singh, E. Kendrick, J. Stowell, B. Taylor, and S. Calmantl, 2002, Geodetic observations of very rapid convergence and back-arc extension at the Tonga arc, *Nature*, v 374, 249-251, doi: 10.1038/374249a0
- Bird, P., 2003, An updated digital model of plate boundaries, *Geochemistry Geophysics Geosystems*, v 4, p 1-52.
- Bonnardot, M.-A., M. Regnier, C. Christova, E. Ruellan, and E. Tric, 2009, Seismological evidence for a slab detachment in the Tonga subduction zone, *Tectonophysics*, v 464, p 84-99.
- Calmant, S., B. Pelletier, P. Lebellegard, M. Bevis, F. W. Taylor, D. A. Phillips, 2003, New insights on the tectonics along the New Hebrides subduction zone based on GPS results, *Jour. Geophys. Res.*, v 108, p. 2319-2342, doi: 10.1029/2001JB000644.
- Christova, C. and C.H. Scholz, H. Kao, 2003, Stress field in the Vanuatu (New Hebrides) Wadati-Benioff zone inferred by inversion of earthquake focal mechanisms: evidence for systematic lateral and vertical variations of principal stresses, 2004, *J. Geodynamics*, v 37, p 125-137.
- Cleveland, M., C. J. Ammon, and T. Lay, 2010, Interacting earthquakes along the northern Vanuatu subduction zone, American Geophysical Union, Fall meeting 2010.

- DeMets, C., R. G. Gordon, D. F. Argus, and S. Stein, 1994, Effect of recent revisions to the geomagnetic reversal time scale on estimate of current plate motions, *Geophys. Res. Lett.*, 21, 2191-2194.
- Engdahl, E.R., and Villaseñor, A., 2000,. Global seismicity—1900–1999, *in* Lee, W.H.K., Kanamori, H., Jennings, P.C., and Kisslinger, C., eds., *International Handbook of Earthquake and Engineering Seismology*, International Association of Seismology and Physics of the Earth's Interior (IASPEI), p. 665–690.
- Frankel, A.D., M.D. Petersen, C.S. Mueller, K.M. Haller, R.L. Wheeler, E.V. Leyendecker, R.L. Wesson, S.C. Harmsen, C.H. Cramer, D.M. Perkins, K.S. Rukstales, 2002, Documentation for the 2002 Update of the National Seismic Hazard Maps, USGS Open-file report 02-420.
- Frankel, A., 1995, Mapping seismic hazard in the Central and Eastern United States: Seismological Research Letters, v. 66, p. 8–21.
- Frolich, C., 1989, The nature of deep focus earthquakes, *Ann. Rev. Earth Planet. Sci.*, v.17, p. 227-254.
- Frolich, C., 2001, Display and quantitative assessment of distributions of earthquake focal mechanisms, *Geophys. J. Int* (2001, v 144, p 300-308.
- Gardner, J.K., and Knopoff, L., 1974, Is the sequence of earthquakes in southern California, with aftershocks removed, Poissonian?, *Bull. Seismol. Soc. Amer.*, v. 64, p. 1363-1367.
- Giardini, D., 1999, The global seismic hazard assessment program (GSHAP) – 1992-1999, *Annali di Geofisica*, V 42, p 957-974.
- Gutenberg, B., and Richter, C.F., 1944, Frequency of earthquakes in California, *Bull. Seismol. Soc. Amer.*, v. 34, p. 185–188.
- Hayes, G.C., D. J. Wald, and R. L. Johnson, 2011, Introducing Slab1.0, a three-dimensional model of global subduction zone geometries, preprint, <http://earthquake.usgs.gov/research/data/slab/>

- Jaffe, B.E., Gelfenbaum, Guy, Buckley, M.L., Watt, Steve, Apotsos, Alex, Stevens, A.W., and Richmond, B.M., 2010, The limit of inundation of the September 29, 2009, tsunami on Tutuila, American Samoa: U.S. Geological Survey, Open-File Report OF-2010-1018, scale 1:222200.
- McNamera, D. E., Petersen, M. D., Meremonte, M. E., Fox, J, Leeds, A., 2009, Ground motions from the 29 September 2009 Samoa M 8.0 earthquake and aftershocks, American Geophysical Union, Fall Meeting 2009, <http://adsabs.harvard.edu/abs/2009AGUFM.U21D..02M>.
- Okal, E. A., Borreo, J., and Synolakis, C. E., 2004, The earthquake and tsunami of 1865 November 17: evidence for far-field tsunami hazard from Tonga, *Geophys. J. Int.*, v 157, p 164-174.
- Petersen, M.D, Frankel, A.D, Harmsen, S.C., Mueller, C.S., Haller, K.M., Wheeler, R.L., Wesson, R.L., Zeng, Y., Boyd, O.S., Perkins, D.M., Luco, N., Field, E.H., Wills, C.J., and Rukstales K.S., 2008, Documentation for the 2008 Update of the United States National Seismic Hazard Maps, USGS Open-File Report 2008-1128, 60 pp, 11 appendices.
- Pelletier, B., S. Calmant, and R. Pillet, 1998, Current tectonics of the Tonga-New Hebrides region, *Earth and Planetary Science Letters*, v 164, p 263-276.
- Prevot, R., J-L. Chatelain, S.W. Roecker, and F-R. Grasso, 1994, A shallow double seismic zone beneath the central New Hebrides (Vanuatu): evidence for fragmentation and accretion of the descending plate?, *Geophys. Res. Lett.*, v 21, p 2159-2162.
- Satake, K., 2010, Earthquakes: double trouble at Tonga, *Nature*, v 466, p 931-932.
- Sipkin, S.A., 2003, A correction to body-wave magnitude mb based on moment magnitude Mw, *Seismological Research Letters*, v. 74, p. 739-742.
- Utsu, T., 2002, Relationships between magnitude scales, *in* Lee, W.H.K., Kanamori, H., Jennings, P.C., and Kisslinger, C., eds., *International Handbook of Earthquake and Engineering Seismology*, International Association of Seismology and Physics of the Earth's Interior (IASPEI), p. 733-746.

Wessel, P., and W.H.f. Smith, 2004, The Generic Mapping Tools (GMT) version 4 Technical Reference & Cookbook, SOEST/NOAA.

Youngs, R. R., Chiou, S.-J., Silva, W.J., and Humphrey, J. R., 1997, Strong ground motion attenuation relationships for subduction zone earthquakes, *Seismol. Res. Lett.*, v 68, 1997.

Zhao, J.X., Zhang, J., Asano, A., Ohno, Y., Oouchi, T., Takahashi, T., Ogawa, H., Iridura, K., Thio, H. K., Somerville, P. G., Fukushima, Y., and Fukushima, Y., 2006, Attenuation relations of strong ground motion in Japan using site classification based on predominant period, *Bull. Seismol. Soc. Amer.*, v 96, 898-913.

Acknowledgements

We thank Antonio Villisenior, Gavin Hayes, Emile Okale, George Choy, and Nico Luco for constructive discussions that were critical for our analysis. We also thank Art Frankel for thoughtful reviews of the manuscript. This work was done to support the NEHRP Recommended Provisions for Seismic Regulations building codes for American Samoa.

Appendix A: Lessons of the Samoa from the M8.3 Tokachi-Oki and the M9 Tohoku Earthquakes

Stephen Harmsen

The ideal data set for predicting future ground motions in American Samoa from Tonga-Kermadec subduction events would be extensive strong-motion recordings of past Tonga-Kermadec subduction events for a range of distances and event magnitudes that span the expected events. However, such data are extremely sparse. We examined Global Digital Seismic Network (GDSN) records from several Pacific Ocean trench regions, including Tonga and Kermadec, and found several that either are or are suspected to be from oceanic-plate-subduction events. The criteria for considering the event subduction are that they are relatively shallow (hypocenters in the 0 to 50 km range), with epicenters in the subducting slab region and Harvard moment tensor solutions with strongly reverse-slip motion. We recognize that these criteria are more in the necessary category than the sufficient category. The 1-s spectral acceleration data from such events are shown in figure A0, and are compared with Zhao and others (2006) subduction event predictions for sources having magnitude in the range $6 < M < 8$. The curves in fig. A0 are based on an assumed site condition of 600 m/s. The data are from stations that are generally located on volcanic rock outcrops. Figure A0 shows that there are too few GDSN data to provide strong constraints on which model or models to use for predicting ground motions. As is commonly done in PSHA studies, we study information from similar, but distant, tectonic environments to try to guide our choice of models for predicting American Samoa ground motions.

Zhao et al. Interface & GDSN Data

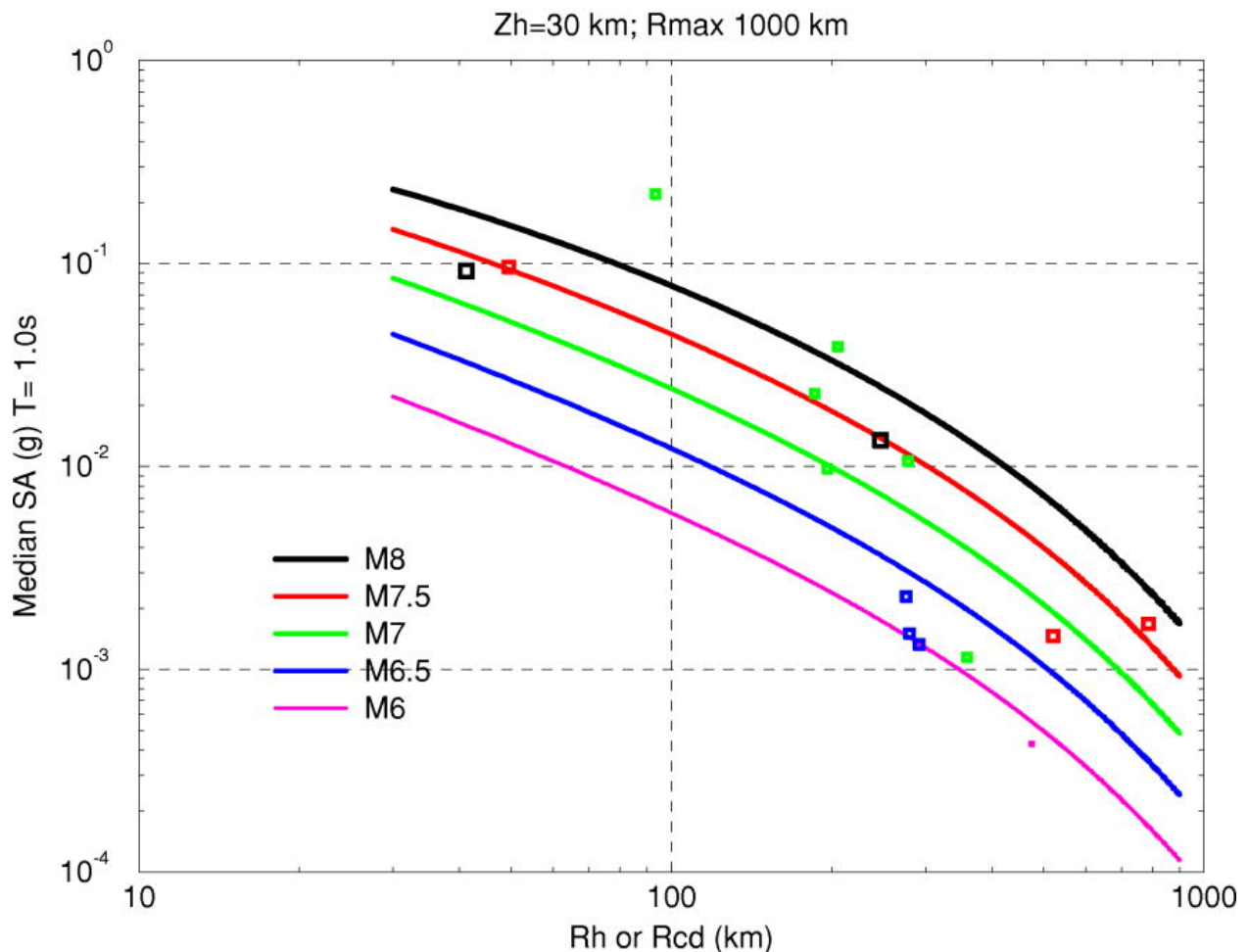


Figure A0. 1-s spectral acceleration (SA) data from Global Digital Seismic Network (GDSN) for known or suspected interface earthquakes and predictions of SA from the Zhao and others (2006) model. Data and model correspond to the geometric mean of the peak motions on the two horizontal-component response functions.

Tokachi-Oki Earthquake of September 26, 2003

The Tokachi-oki mainshock was well recorded by Japan's KiKNet and KNet seismograph networks with at least 360 stations providing usable seismograms. Japan's dense KiKNet and K-Net seismograph networks were installed beginning in 1996 following the 1995 Hyogoken-nanbu (Kobe) earthquake. Tokachi-Oki seismograms were processed to supply spectral response and peak ground velocity, with results available at the USGS Shake Map URL, <http://earthquake.usgs.gov/earthquakes/shakemap/atlas/shake/200309251950/>, last accessed May 4, 2011. To compare the motions with available ground-motion prediction equations, or GMPEs, we need a geometry model of the part of the plate interface that ruptured during that earthquake. In the below figures we use the rupture model of Kamae and Kawabe (2004) to infer closest distance, r_{cd} . In their model, the rupture surface has length 128 km and width 80 km. Its dip is 26° . For comparison, the Geomatrix (1995?) expected length of an M8.3 subduction source is 261 km. The compactness of the source may in part be due to its relatively great width, with an aspect ratio of 1.6. Many subduction sources may be expected to have aspect ratios of 2.5 or greater. We use the Geomatrix expected length to predict rupture length of M7 to M9 subduction events on the Tonga-Kermadec and New Hebrides interfaces.

Figure A1 shows the Tokachi-oki PGA data (geometric mean of the two horizontal components) and three GMPEs for subduction events with M8.3, assuming a uniform 600 m/s site condition, i.e., NEHRP Class C soil classification. In the 200 to 300 km range, where predictions are important to the American Samoa seismic hazard, these models tend to over predict the motion, with the Zhao and others (2006) model exhibiting the least bias. Site condition for most of these data is NEHRP Class C, D, or E soil, reported at the URL <http://www.k-net.bosai.go.jp/>. Given these site conditions, a factor of two (\pm) soil amplification compared to rock at the same location is to be expected. The curves, which correspond to a very stiff soil or firm rock, are clearly biased high compared to Tokachi-oki data scaled to a common site condition of 600 m/s V_{s30} , at distances in the 200-500 km range.

Tokachi-Oki Main Shock Sept 26, 2003

3 GMPEs for M8.3 subduction. Site Vs30 600 m/s

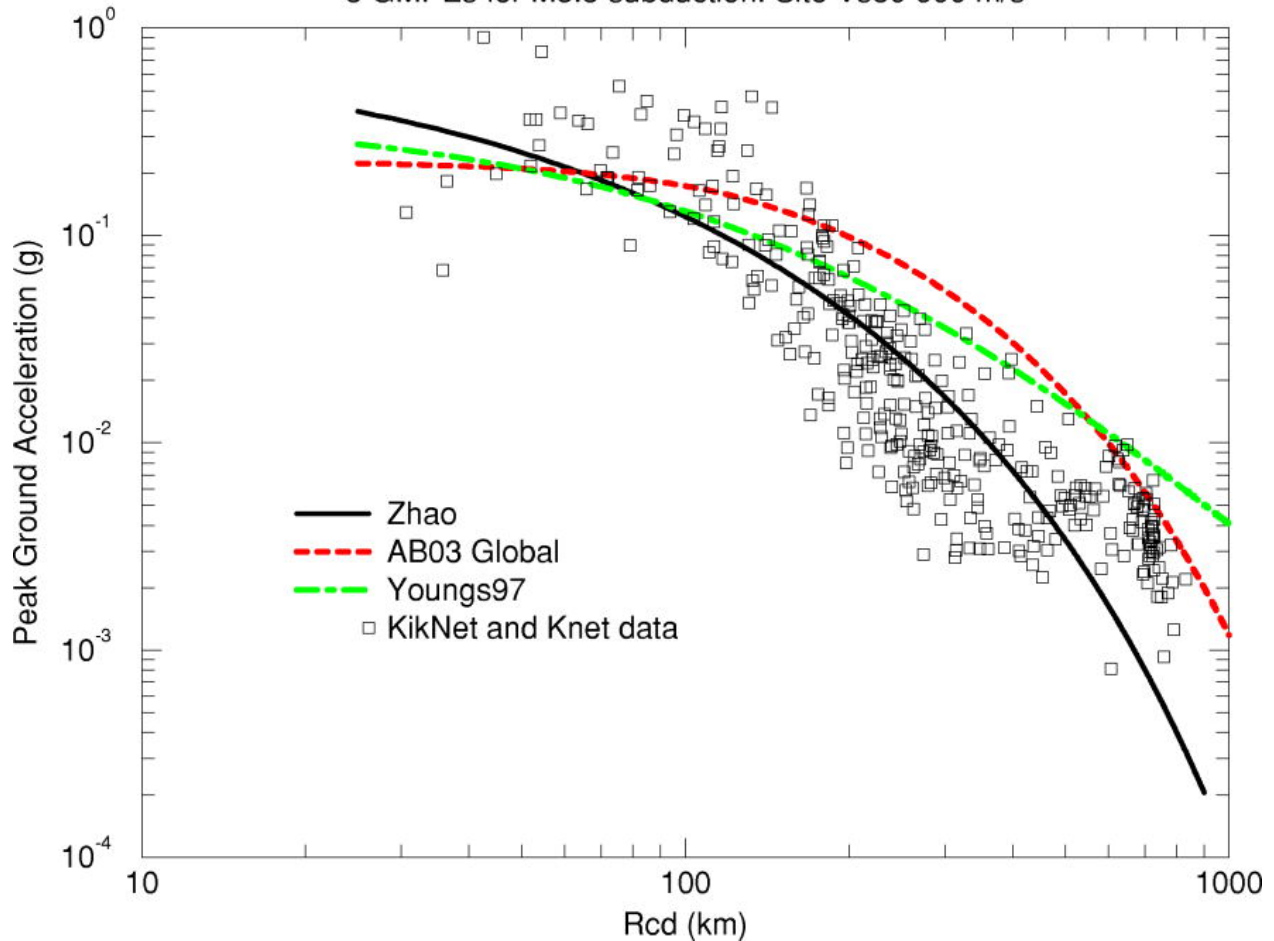


Figure A1. Tokachi-Oki main shock data and three ground motion models for peak ground acceleration from subduction source with M8.3 and depth 25 km. The data are mostly from sites located on soil with NEHRP site class C, D, and E. The curves, however, correspond to an upper-C site class.

Figure A2 shows the 0.3-s spectral acceleration data and three GMPE models, again computed for a 600 m/s site condition. The 0.3-s data are here used as a proxy for 0.2-s data, because 0.2-s data are not available at the Shake Map web site, but seismic hazard at 0.2-s period is discussed in this article. Stations in the Tokyo subnet of K-Net are highlighted in red. These Tokyo stations are on thin to thick soil, often NEHRP class D or even E, as are most other K-Net stations. In the 200 to 300 km range, these GMPEs tend to over predict the data, especially when a factor of two (\pm) is divided out to remove expected soil amplification. The Zhao and others (2006) GMPE clearly exhibits the least high bias in that distance range.

Tokachi-Oki Main Shock Sept 26, 2003

3 GMPEs for M8.3 subduction. Site Vs30 600 m/s

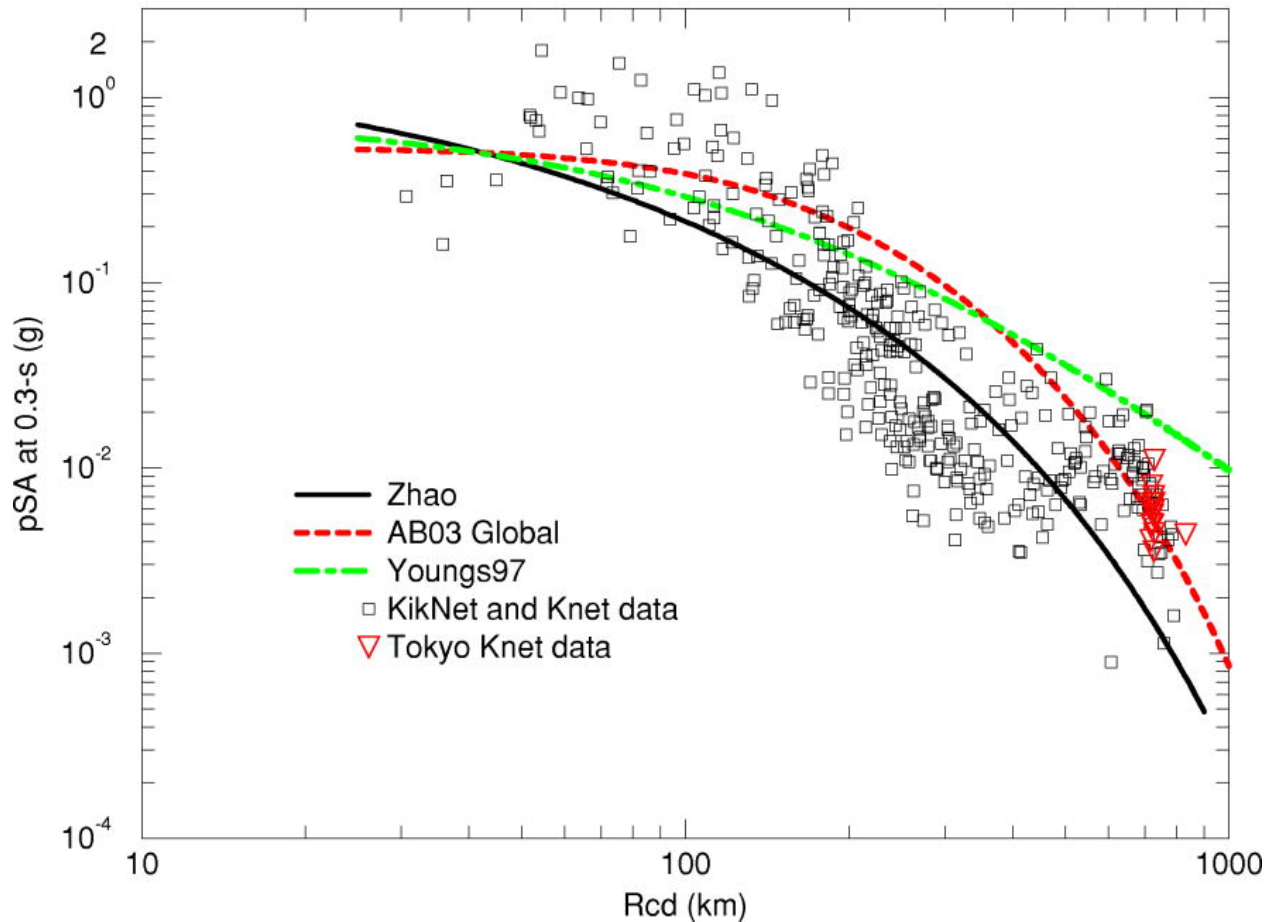


Figure A2. Tokachi-Oki main shock data and three ground motion models for pseudo spectral acceleration (pSA) at 0.3-s period (5% damping) from subduction source with M8.3 and depth 25 km. The data are mostly from sites located on soil with NEHRP site class C, D, and E. The curves, however, correspond to an upper-C site class.

Figure A3 below shows the Tokachi-Oki ground motion data and three GMPEs for 1-s spectral acceleration. The data correspond to soil sites, and if they are reduced by a factor of two (\pm) to remove soil amplification, they tend to fall below the curves in the important distance range of 200 to 500 km. Again, the Zhao and others (2006) model tends to have the smallest bias in this distance range. The models have comparable amplitudes in the near source distance range ($R_{cd} < 100$ km).

Tokachi-Oki Main Shock Sept 26, 2003

3 GMPEs for M8.3 subduction. Site Vs30 600 m/s

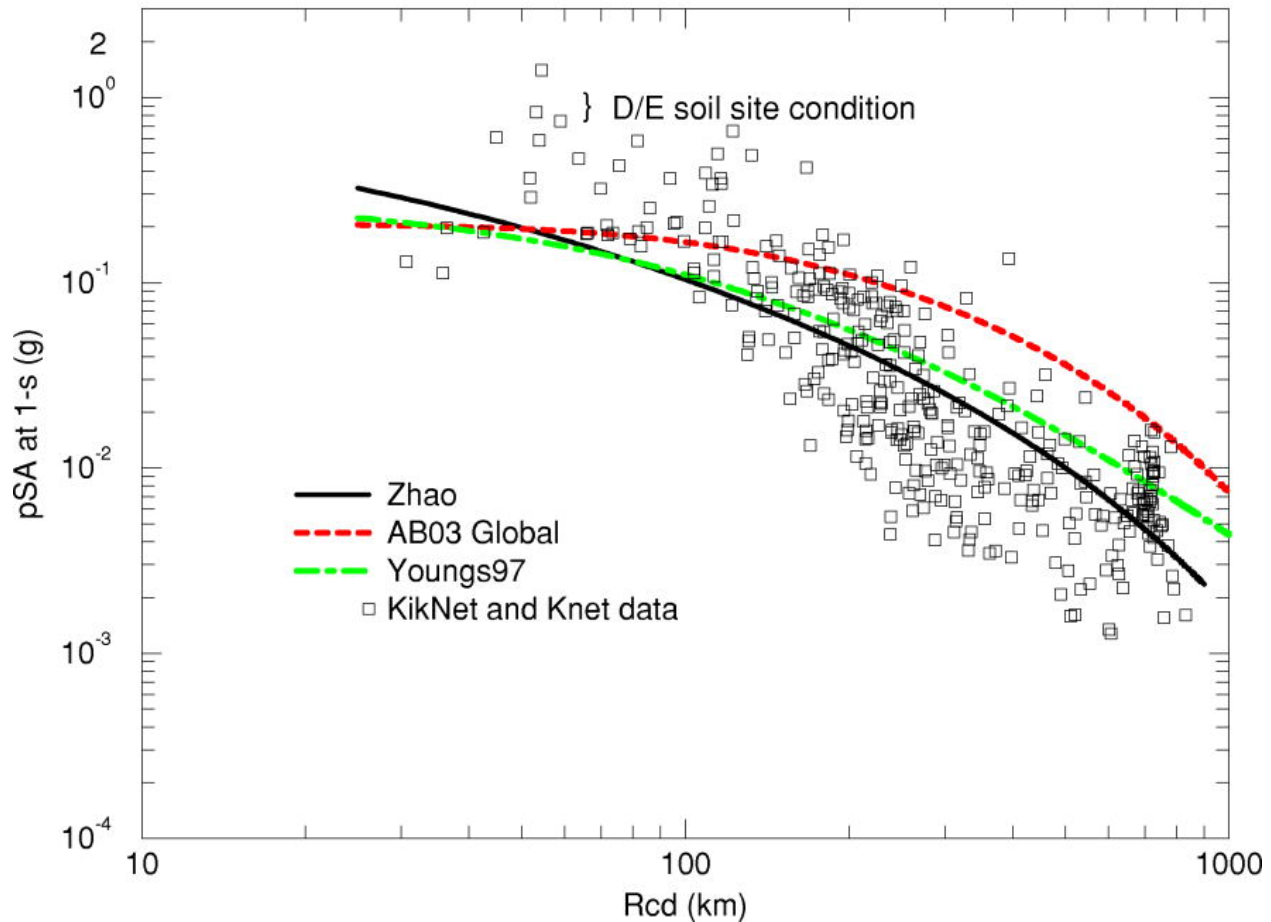


Figure A3. Tokachi-Oki main shock data and three ground motion models for pseudo spectral acceleration (pSA) at 1.0-s period (5% damping) from subduction source with M8.3 and depth 25 km.

Tohoku Earthquake of March 11, 2011

Besides the obvious lesson that M9 subduction events produce large destructive tsunamis, often with columns of water having 10 m depth rushing inland and destroying everything and everyone in their path, the Tohoku earthquake provides valuable information about ground acceleration at a broad range of distances as recorded on a variety of soil and rock sites. Approximately 1200 K-Net and KiKNet instruments provided useful seismograms from the Tohoku earthquake. These seismograms were processed to supply spectral response and peak ground velocity, with results available at the USGS Shake Map URL, <http://earthquake.usgs.gov/earthquakes/eqinthenews/2011/usc0001xgp/>, last accessed May 4, 2011. To compare the motions with available ground-motion prediction equations, or GMPEs, we need a geometry model of the part of the plate interface that ruptured during that earthquake. In the below figures we use the rupture model of Gavin Hayes, USGS, which has length 621 km and width 254 km. The Hayes model is more fully described at URL, http://earthquake.usgs.gov/earthquakes/eqinthenews/2011/usc0001xgp/finite_fault.php. For comparison, the Geomatrix expected length of an M9 megathrust event is 833 km. The shorter length of the Tohoku rupture according to the Hayes model is more than compensated by the greater than usual width, which corresponds to a very gentle interface dip of about 10°. The Tonga trench interface has a much steeper dip, and is expected to produce relatively long ruptures for a given magnitude.

Most of the stations in Japan's KiKNet network are located on sedimentary rock or on thin soil over sedimentary rock, and correspond, more often than not, to the NEHRP Class C geotechnical site class, $350 < V_{s30} < 600$ m/s. Most of the stations in the K-Net network are located on thin to thick sediment over sedimentary rock, and mostly correspond to NEHRP Class E

(120 to 180 m/s) and Class D (180 to 350 m/s) site classes. Detailed geotechnical logs are available for many of these KNet stations at URL <http://www.k-net.bosai.go.jp/>. This report, however, primarily focuses on seismic hazard corresponding to rock at the NEHRP B/C interface, with $V_{s30} = 760$ m/s. When comparing prediction curves with data, we choose a uniform 600 m/s rock site condition, which is a compromise between the data and the American Samoa modeling work. Figure A4 below shows the PGA data (geometric mean of the two horizontal components) and three GMPE models. The data generally plot below the models except at near-source distances, where several data plot two to three times above the prediction. If we could remove site response from the data, they would tend to plot even further below the predictions, except at relatively near-source distances, where they would be close to the predictions. For sites in American Samoa, the distance to the Tonga-interface source is about 200 -250 km. Samoa does not lie in the direction of slip. Pago Pago and the rest of American Samoa are northeast of the trench, just as Tokyo is southwest of the Tohoku rupture, although only 60 km or so distant. Tokyo KNet data are plotted as red triangles in fig. A4. Figure A4 clearly shows that of the three GMPEs we have been considering, only the Zhao 2006 model does a reasonably good job of fitting the data in the inner 300 km (the Zhao model was not designed to fit data beyond 300 km).

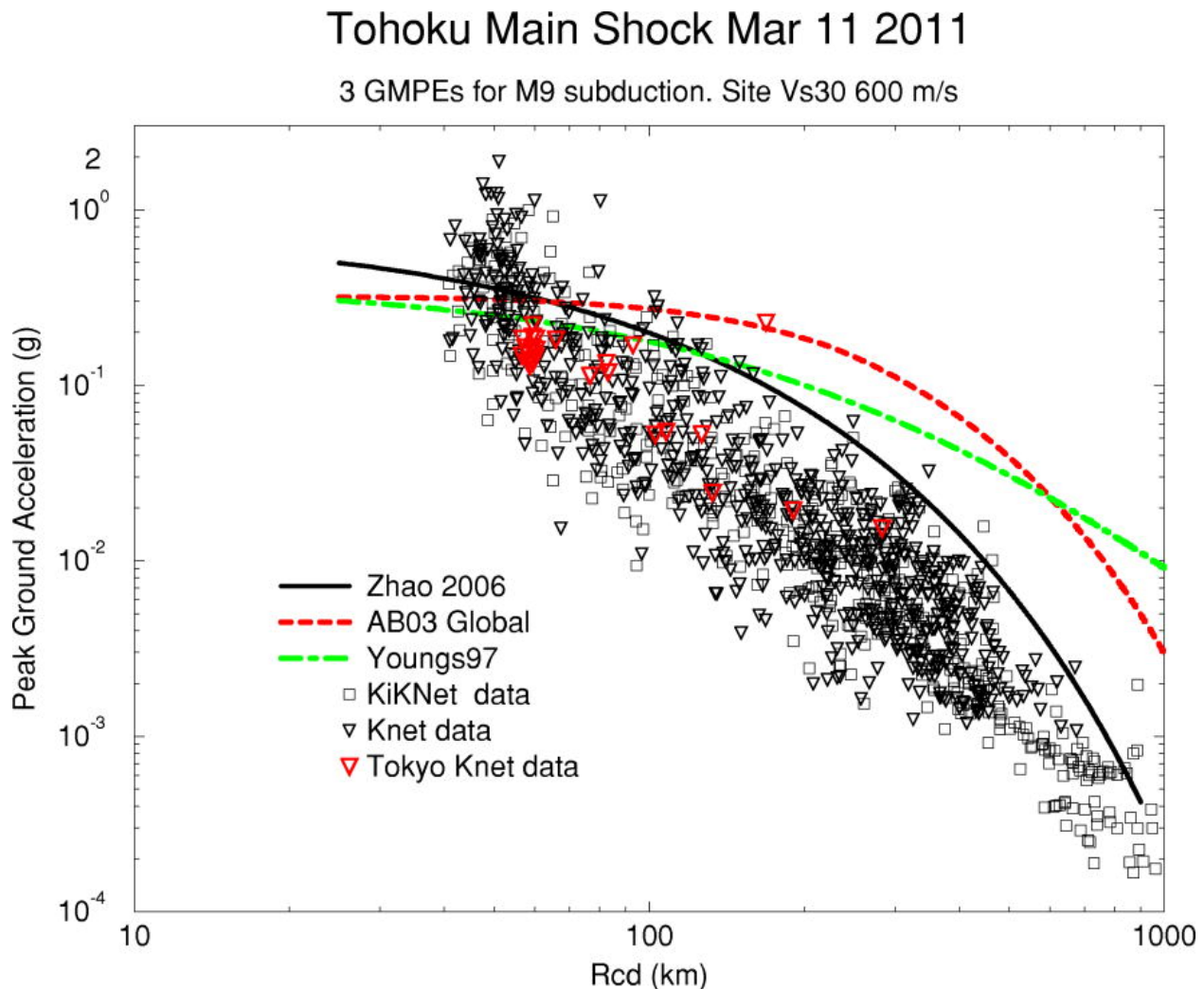


Figure A4. Peak ground acceleration models and data for an M9 megathrust earthquake.

Figure A5 below shows the 0.3-s Tohoku data (geometric mean of the two horizontal components) and three subduction GMPEs. As in fig. A4, the Zhao 2006 model outperforms the others in goodness-of-fit. These data tend to justify the exclusive use of the Zhao 2006 model, given these three GMPEs to choose among. This we have done in this seismic-hazard report. Data corresponding to 0.2-s spectral period were not available from the Shake Map web site, so we are substituting these 0.3-s spectral period data and expecting the same behavior for 0.2-s data.

Tohoku Main Shock Mar 11 2011

3 GMPEs for M9 subduction. Site Vs30 600 m/s

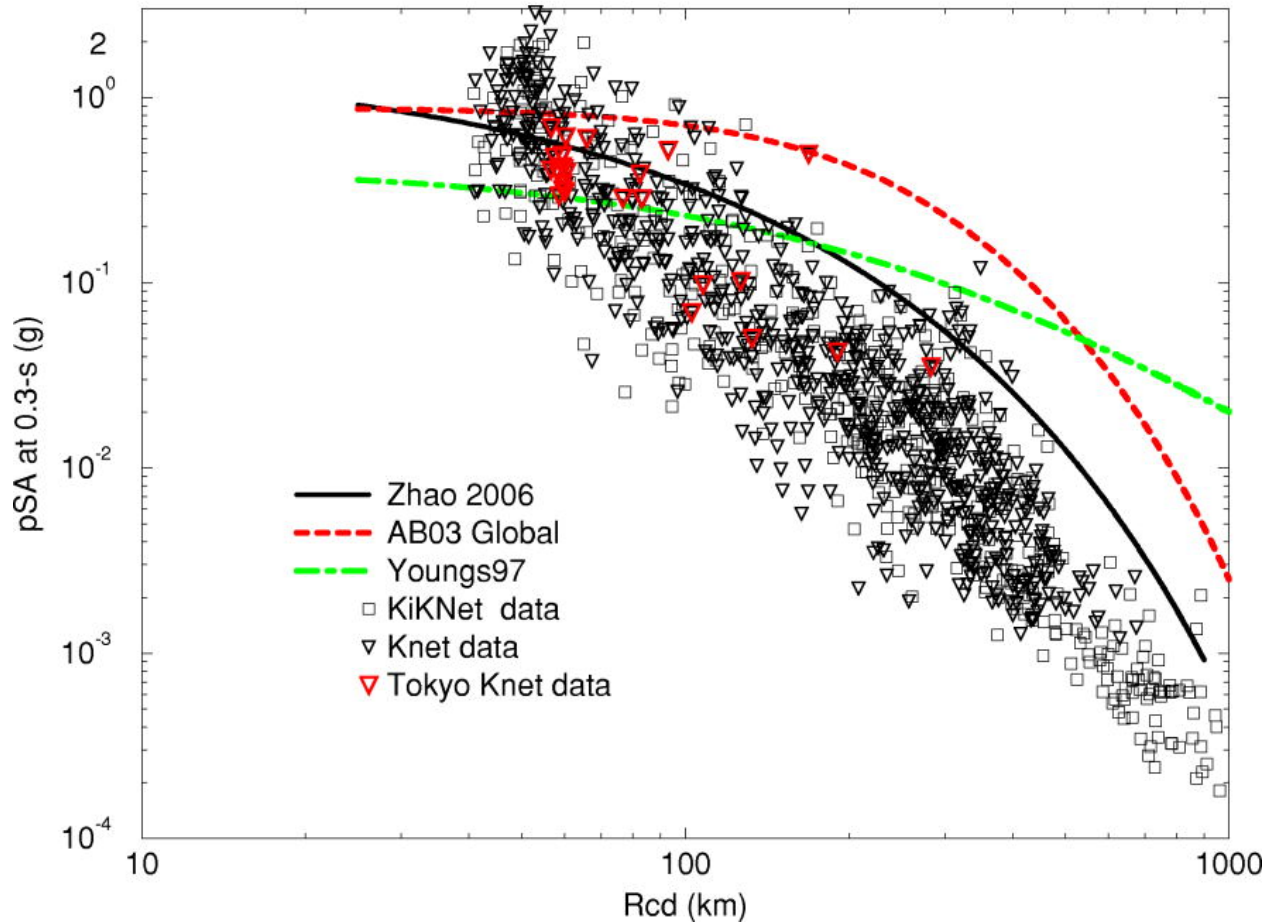


Figure A5. Data and GMPEs for 0.3-s pseudo spectral acceleration (pSA). Rcd is the closest distance from the site to the rupture surface.

Figure A6 below shows the 1.0-s Tohoku data (geometric mean of the two horizontal components) and three GMPEs for an M9 interface earthquake. As usual, the Zhao 2006 model clearly outperforms the others at most distances and this plot tends to justify the exclusive use of the Zhao 2006 model with subduction-source branches of the logic tree.

Tohoku Main Shock Mar 11 2011

3 GMPEs for M9 subduction. Site Vs30 600 m/s

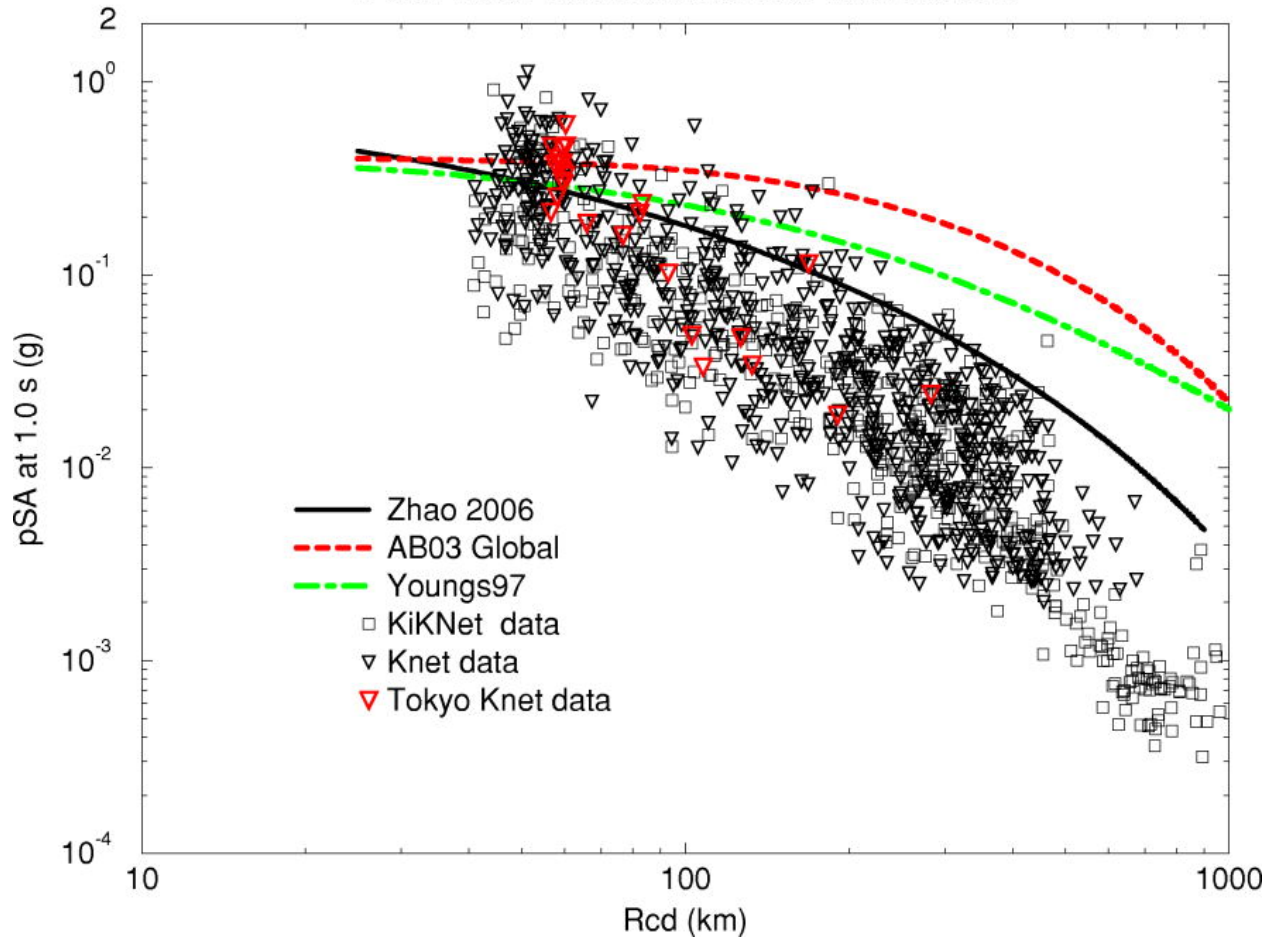


Figure A6. Data and GMPEs for 1.0-s pseudo spectral acceleration (pSA). Rcd is the closest distance from the site to the rupture surface.

The extensive KiKNet and K-Net data from the M9 Tohoku earthquake fill in a big gap in strong motion data from megathrust events. Questions remain about the applicability of these data to other tectonic plates with their unique rock properties, slab dips and convergence rates. Still, we believe data from similar events and tectonic environments are preferable to none as aids when making decisions about models to use in the American Samoa PSHA.

Conclusion

Figures A1 to A6 strongly suggest that there is no basis for raising the Zhao curve from the predicted value the way we have done for PGA and for 0.2-s SA associated with intraplate sources. For interface source ground-motion prediction, we use the Zhao and others (2006) model as published, with 25% uncertainty branches on the mean when $M < 8.5$, and 50% uncertainty branches on the mean when $M \geq 8.5$. This additional epistemic uncertainty is used as a substitute for alternate published GMPEs, which we found less appropriate for modeling the data sets we studied.

Reference:

Kamae, K. and H. Kawabe (2004). Source model composed of asperities for the 2003 Tokachi-oki, Japan, earthquake ($M_{JMA}=8.0$) estimated by the empirical Green's function method. *Earth Planets Space*, v 56, pp. 323-327.